


RESEARCH ARTICLE

Biocompatibility of Subcutaneously Implanted Plant-Derived Cellulose Biomaterials

Daniel J. Modulevsky^{1,2} , Charles M. Cuerrier^{1,3} , Andrew E. Pelling^{1,2,3,4,5*}

1 Centre for Interdisciplinary NanoPhysics, University of Ottawa, Ottawa, Ontario, Canada, **2** Department of Biology, University of Ottawa, Ottawa, Ontario, Canada, **3** Department of Physics, University of Ottawa, Ottawa, Ontario, Canada, **4** Institute for Science, Society and Policy, University of Ottawa, Ottawa, Ontario, Canada, **5** SymbioticA, School of Anatomy, Physiology and Human Biology, University of Western Australia, Perth WA 6009, Australia

 These authors contributed equally to this work.

* a@pellinglab.net.



 OPEN ACCESS

Citation: Modulevsky DJ, Cuerrier CM, Pelling AE (2016) Biocompatibility of Subcutaneously Implanted Plant-Derived Cellulose Biomaterials. PLoS ONE 11 (6): e0157894. doi:10.1371/journal.pone.0157894

Editor: Feng Zhao, Michigan Technological University, UNITED STATES

Received: February 12, 2016

Accepted: June 7, 2016

Published: June 21, 2016

Copyright: © 2016 Modulevsky et al. This is an open access article distributed under the terms of the [Creative Commons Attribution License](https://creativecommons.org/licenses/by/4.0/), which permits unrestricted use, distribution, and reproduction in any medium, provided the original author and source are credited.

Data Availability Statement: All relevant data are within the paper.

Funding: This study was funded by a Natural Sciences and Engineering Resource Council (NSERC) Discovery Grant (#RGPIN-2014-04978) and the University of Ottawa Faculty Development Fund. D.J.M. was supported by a graduate student fellowship from the "Fonds de Recherche du Québec — Santé" (FRQS). C.M.C. was supported by a postdoctoral training award from the "Fonds de Recherche du Québec — Santé" (FRQS). A.E.P. would like to acknowledge generous support from the Canada Research Chairs Program (#950-229071). The funders had no role in study design, data

Abstract

There is intense interest in developing novel biomaterials which support the invasion and proliferation of living cells for potential applications in tissue engineering and regenerative medicine. Decellularization of existing tissues have formed the basis of one major approach to producing 3D scaffolds for such purposes. In this study, we utilize the native hypanthium tissue of apples and a simple preparation methodology to create implantable cellulose scaffolds. To examine biocompatibility, scaffolds were subcutaneously implanted in wild-type, immunocompetent mice (males and females; 6–9 weeks old). Following the implantation, the scaffolds were resected at 1, 4 and 8 weeks and processed for histological analysis (H&E, Masson's Trichrome, anti-CD31 and anti-CD45 antibodies). Histological analysis revealed a characteristic foreign body response to the scaffold 1 week post-implantation. However, the immune response was observed to gradually disappear by 8 weeks post-implantation. By 8 weeks, there was no immune response in the surrounding dermis tissue and active fibroblast migration within the cellulose scaffold was observed. This was concomitant with the deposition of a new collagen extracellular matrix. Furthermore, active blood vessel formation within the scaffold was observed throughout the period of study indicating the pro-angiogenic properties of the native scaffolds. Finally, while the scaffolds retain much of their original shape they do undergo a slow deformation over the 8-week length of the study. Taken together, our results demonstrate that native cellulose scaffolds are biocompatible and exhibit promising potential as a surgical biomaterial.

Introduction

The development of novel biomaterials for tissue engineering strategies is currently under intense investigation [1–3]. Biomaterials are being developed for the local delivery of therapeutic cells to target tissues [4,5], the regeneration of damaged or diseased tissues [6–9] or the replacement of whole organs [10–15]. In their most general form, biomaterials provide a three-

collection and analysis, decision to publish, or preparation of the manuscript.

Competing Interests: Andrew E. Pelling is a PLOS ONE Editorial Board member. The authors explicitly state herein that, by acting as a member of the editorial board of PLOS ONE, this does not alter the authors' adherence to all the PLOS ONE policies on sharing data and materials.

dimensional (3D) scaffold which attempts to mimic the *in vivo* cellular milieu [14,16]. Approaches have been developed to engineer the mechanical [17–24], structural [25] and biochemical properties [26–29] of these scaffolds with varying complexity. As well, significant efforts are underway to ensure that such implanted biomaterials are biocompatible and stimulate only minimal immune responses. The efforts in biomaterials research is being driven by the significant need for replacement organs and tissues. With an aging population, the gap between patients waiting for organ transplants and available donor organs is rapidly increasing [30]. While clinical applications of biomaterials have been somewhat limited, physicians have successfully utilized synthetic biomaterials to treat various damaged tissues and structures, such as skin, gum, cartilage, and bone [31–36].

Biomaterial scaffolds can take several forms such as powders, gels, membranes, and pastes [1,2]. Such polymer or hydrogel formulations can be moulded or 3D-printed to produce forms that are of therapeutic values [37–39]. An alternative approach to these synthetic strategies is whole organ decellularization [10,12–16]. Indeed, it has been shown that it is possible to dissociate the cells from a donated organ, leaving behind the naturally occurring scaffold matrix, commonly referred as a ghost organs [14]. The ghost organs lack any of the cells from the donor and can be subsequently cultured with cells derived from the patient or another source. Such approaches have already been utilized to repair and replace defective tissues [40–42]. In the past several years, many body parts have been created using synthetic and decellularization approaches, including the urethra, vaginal, ear, nose, heart, kidney, bladder, and neurological tissues [14,38,39,43–47].

However, these approaches are not without some disadvantages [48]. Synthetic techniques can require animal products and decellularization strategies still require donor tissues and organs. There has also been intense investigation into the development of resorbable biomaterials [49]. In these cases, the aim is to provide the body with a temporary 3D scaffold onto which healthy tissues can form. After several weeks or months, the implanted scaffold will be resorbed leaving behind a completely natural healthy tissue [26,29,50,51]. Although this is an ideal approach, many non-resorbable biomaterials (ceramic, titanium) have been successfully employed in clinical settings and play a major role in numerous therapies [2,49,52–57]. Importantly, resorbable biomaterials suffer from the fact that regenerated tissues often collapse and become deformed due to the loss of structure [58–62]. For example, for several decades, research on ear reconstruction from engineered cartilage has shown that biomaterial implants eventually collapse and become deformed as the implanted scaffolds break down and resorb [63]. However, recent successful approaches have relied on the use of resorbable collagen scaffolds embedded with permanent titanium wire supports [53,64,65]. Therefore, the need for non-resorbable, yet biocompatible, scaffolds persists in the field of tissue and organ engineering.

Recent complementary approaches have utilized scaffolding materials that are not derived from human organ donors or animal products. Namely, various forms of cellulose have been shown to have utility in both *in vitro* and *in vivo* studies [66–71]. Cellulose is abundant in nature, is easily produced and sourced, can be chemically modified to control surface biochemistry and produced as hydrogels with tuneable porosity and mechanical properties [67,72–77]. Moreover, nanocrystalline, nanofibrillar and bacterial cellulose constructs and hydrogels also have been shown to support the proliferation and invasion of mammalian cells *in vitro* and *in vivo* with high biocompatibility [78–83]. In our recent work, we developed an orthogonal, yet complementary, approach to organ decellularization and synthetic cellulose strategies. We developed a highly robust and cost effective strategy for producing cellulose biomaterials from decellularized apple hypanthium tissue [27]. The scaffolds required no further complex processing as is often the case in the production of nanocrystalline, nanofibrillar and bacterial

cellulose constructs. The cellulose scaffolds were employed for *in vitro* 3D culture of NIH3T3 fibroblasts, mouse C2C12 muscle myoblasts and human HeLa epithelial cells. Our previous work revealed that these cells could adhere, invade and proliferate within the cellulose scaffolds and retain high viability even after 12 continuous weeks of culture.

Our previous work opens the question of *in vivo* biocompatibility [27]. Therefore, the objective of this study is to characterize the response of the body to apple-derived cellulose scaffolds. Macroscopic ($\sim 25\text{mm}^3$) cell-free cellulose biomaterials were produced and subcutaneously implanted in mouse model for 1, 4 and 8 weeks. Here, we assess the immunological response of immunocompetent mice, deposition of extracellular matrix on the scaffolds and evidence of angiogenesis (vascularization) in the implanted cellulose biomaterials. Notably, although a foreign body response was observed immediately post-implantation, as expected for a surgical procedure, by the completion of the study only a low immunological response was observed with no fatalities or noticeable infections whatsoever in all animal groups. Surrounding mouse cells were also found to invade the scaffold, mainly activated fibroblasts, and deposit a new extracellular matrix. As well, the scaffold itself was able to retain much of its original shape and structure over the 8-week study. Importantly, the scaffolds clearly had a pro-angiogenic effect, resulting in the growth of functional blood vessels throughout the implanted biomaterial. Taken together, our work demonstrates that we can easily produce 3D cellulose scaffolds that are biocompatible, becoming vascularized and integrated into surrounding healthy tissues.

Material and Methods

Animals

All experimental procedures were approved by the Animal Care and Use Committee of the University of Ottawa. Wild-type C57BL/10ScSn mice (males and females; 6–9 weeks old; $n = 7$ mice for each group) were purchased from The Jackson Laboratory (Bar Harbor, Maine, USA) and bred in our facilities. All animals were kept at constant room temperature ($\pm 22^\circ\text{C}$) and humidity ($\sim 52\%$). They were fed a normal chow diet and kept under a controlled 12 hours light/dark cycle.

Cellulose scaffold preparation

As described previously [27], McIntosh Red apples (Canada Fancy) were stored at 4°C in the dark for a maximum of two weeks. In order to prepare apple sections, the fruit was cut with a mandolin slicer to a uniform thickness of $1.14 \pm 0.08\text{mm}$, measured with a Vernier caliper. Only the outer (hypanthium) tissue of the apple was used. Slices containing visible ovary-core tissue were not used. The slices were then cut parallel to the direction of the apple pedicel into squares segments of $5.14 \pm 0.21\text{mm}$ in length and with an area of $26.14 \pm 1.76\text{mm}^2$. Apple tissue was decellularized using a well-established protocol [14] for removal of cellular material and DNA from tissue samples while leaving behind an intact and three-dimensional scaffold. Individual apple tissue samples were placed in sterilized 2.5ml microcentrifuge tubes and 2ml of 0.1% sodium dodecyl sulphate (SDS; Sigma-Aldrich) solution was added to each tube. Samples were shaken for 48 hours at 180 RPM at room temperature. The resultant cellulose scaffolds were then transferred into new sterile microcentrifuge tubes, washed and incubated for 12 hours in PBS (Sigma-Aldrich). The cellulose scaffold were sterilized by incubation in 70% ethanol for 1 hour and then repeatedly washed 12 times with PBS. The samples were then kept in PBS. At this point, the samples were immediately used or stored at 4°C for no more than 2 weeks.

Cellulose implantation

The mice were anesthetized using 2% Isoflurane USP-PPC (Pharmaceutical partners of Canada, Richmond, ON, Canada) with the eyes protected the application of ophthalmic liquid gel (Alco Canada In., ON, Canada). The mouse back hairs were shaved with the underlying skin cleaned and sterilized using ENDURE 400 Scrub-Stat4 Surgical Scrub (chlorhexidine gluconate, 4% solution; Ecolab Inc., Minnesota, USA) and Soluprep (2% w/v chlorhexidine and 70% v/v isopropyl alcohol; 3M Canada, London, ON, Canada). Animal hydration was maintained, via subcutaneous injection (s.c) of 1 ml of 0.9% sodium chloride solution (Hospira, Montréal, QC, Canada). Throughout the surgical procedures all strict sterility measures were upheld for survival surgeries. To implant the scaffolds, two 8mm incisions were cut on the dorsal section of each mouse (upper and lower). Two cellulose scaffold samples were separately and independently implanted into each mouse. The incisions were then sutured using Surgipro II monofilament polypropylene 6-0 (Covidien, Massachusetts, USA) and transdermal bupivacaine 2% (as monohydrate; Chiron Compounding Pharmacy Inc., Guelph, ON, Canada) was topically applied to the surgery sites to prevent infection. Additionally, buprenorphine (as HCL) (0.03mg/ml; Chiron Compounding Pharmacy Inc. Guelph, ON, Canada) was administered s.c. as a pain reliever. All animals were then carefully monitored for the following 3 days by animal care services and received additional treatment of the same pharmacological treatments.

Scaffold resections

At 1, 4 and 8 weeks after scaffold implantation, the mice were euthanized using CO₂ inhalation. After blood collection, the dorsal skin was carefully resected and immediately immersed in PBS solution. The skin sections containing cellulose scaffolds were then photographed, cut and fixed in 10% formalin for at least 48 hours. The samples were then kept in 70% ethanol before being embedded in paraffin by the PALM Histology Core Facility of the University of Ottawa.

Histological analysis

Serial 5µm thick sections were cut, beginning at 1 mm inside the cellulose scaffold, and stained with hematoxylin-eosin (H&E) and Masson's trichrome. For immunocytochemistry, heat induced epitope retrieval was performed at 110°C for 12 min with citrate buffer (pH 6.0). Anti-CD31/PECAM1 (1:100; Novus Biologicals, NB100-2284, Oakville, ON, Canada), anti-alpha smooth muscle actin (1:1000, ab5694, abcam, Toronto, ON, Canada) and anti-CD45 (1:3000; ab10558, abcam, Toronto, ON, Canada) primary antibodies were incubated for a hour at room temperature. Blocking reagent (Background Sniper, Biocare, Medical, Concord, CA, USA) and detection system MACH 4 (Biocare Medical, Concord, CA, USA) were applied according to company specifications. For the evaluation of cell infiltration, extracellular matrix deposition and vascularisation (angiogenesis), micrographs were captured using Zeiss MIRAX MIDI Slide Scanner (Zeiss, Toronto, Canada) equipped with 40x objective and analysed using Panoramic Viewer (3DHISTECH Ltd., Budapest, Hungary) and ImageJ software. The scoring of inflammation was evaluated by a pathologist. The scoring was subjectively assigned by qualitative analysis of the magnitude of the total foreign response as well, the cell population proportions within the foreign response.

Quantification of cellulose volume fraction

To quantitatively determine the average volume of the scaffolds occupied by cellulose H&E images of bare scaffolds were processed according to the following protocol. At least 5 regions of the interest (ROI) of approximate 900µm² were identified in a given H&E image of bare

cellulose. In total we analyzed $n = 5$ H&E images, for a total of 39 ROIs. The area occupied by the cellulose was determined by creating a binary segmented image through thresholding. As each H&E stained section was $5\mu\text{m}$ thick, this allowed us to determine the total volume occupied by cellulose compared to the gross volume of the entire ROI. All image processing was performed with ImageJ 1.47v.

Scanning electron microscopy (SEM)

The structure of cellulose was studied using a scanning electron microscopy. Globally, scaffolds were dehydrated through successive gradients of ethanol (50%, 70%, 95% and 100%). Samples were then gold-coated at a current of 15mA for 3 minutes with a Hitachi E-1010 ion sputter device. SEM imaging was conducted at voltages ranging from 2.00–10.0 kV on a JSM-7500F Field Emission SEM (JEOL, Peabody, MA, USA).

Statistical analysis

All values reported here are the average \pm standard deviations. Statistical analyses were performed with one-way ANOVA by using SigmaStat 3.5 software (Dundas Software Ltd, Germany). A value of $p < 0.05$ was considered statistically significant.

Results

Scaffold Preparation

Cellulose scaffolds were prepared from apple tissue using a modified decellularization technique we have previously described [27]. All scaffolds were cut to a size of $5.14 \pm 0.21 \times 5.14 \pm 0.21 \times 1.14 \pm 0.08\text{mm}$ (Fig 1A), decellularized and prepared for implantation (Fig 1B). The scaffolds appear translucent after decellularization due to the loss of all plant cellular material and debris. The removal of apple cells was also confirmed with histological observation (Fig 1C) and scanning electron microscopy (Fig 1D). Analysis and quantification of the histological images reveals an average cellulose cell wall thickness of $4.04 \pm 1.4\mu\text{m}$, and that the cellulose only occupies $16.9 \pm 3.0\%$ of the total volume of the entire scaffold. The acellular cellulose scaffolds appear to maintain their shape very well and their structure is likely capable of being invaded by nearby cells after implantation in an animal model.

Implantation of Cellulose Scaffolds

Two independent skin incisions (8mm) were produced on the back of each mouse to create small pouches for the biomaterial implantation (Fig 2A). One cellulose scaffold (Fig 2B) was implanted in each subcutaneous pouch. Throughout the study, there were no cases of mice exhibiting any pain behaviour that may have been induced by the cellulose scaffold implantation and none of the mice displayed visible inflammation or infection. The cellulose scaffolds were resected at 1 week, 4 weeks and 8 weeks after their implantation and were photographed to measure the change in scaffold dimensions (Fig 2D–2F). At all-time points, healthy tissue can be observed surrounding the cellulose scaffold with the presence of blood vessels, that are proximal or in direct contact, and the scaffolds retain their square shape. The pre-implantation scaffold had an area of $26.3 \pm 1.98\text{mm}^2$ and it was observed to slowly decrease as function of the implantation time, based on the scaffold area that is visible to the naked eye on the skin (Fig 2G). At 8 weeks post-implantation, the scaffold dimensions reach a near plateau measurement of $13.82 \pm 3.88\text{mm}^2$ demonstrating an approximate 12mm^2 (48%) change over the course of this study.

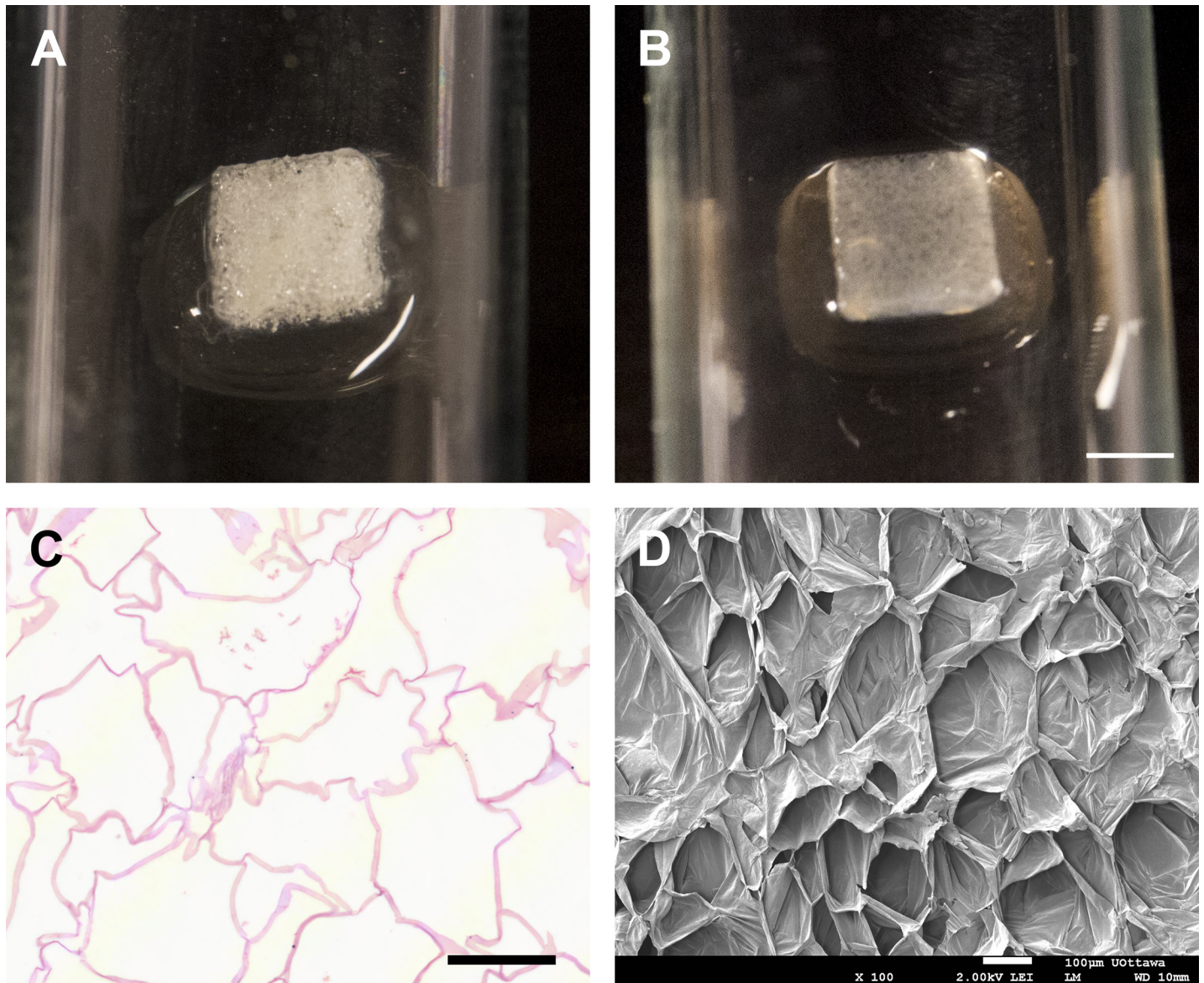


Fig 1. Cellulose scaffold preparation. Macroscopic appearance of a freshly cut apple hypanthium tissue (A) and the translucent cellulose scaffold biomaterial post-decellularization and absent of all native apple cells or cell debris (B). H&E staining of cross sectioned decellularized cellulose scaffold (C). The cell walls thickness and the absence of native apple cells following decellularization are shown. The 3D acellular and highly porous cellulose scaffold architecture is clearly revealed by scanning electron microscopy (D). Scale bar: A-B = 2mm, C-D = 100µm.

doi:10.1371/journal.pone.0157894.g001

Biocompatibility and cell infiltration in plant derived cellulose scaffolds

Scaffold biocompatibility and cell infiltration was examined with H&E staining of fixed cellulose scaffolds at 1, 4 and 8 weeks following their implantation (Fig 3). The global views of longitudinal section of representative cellulose scaffolds are shown in Fig 3A–3C. The scaffolds are implanted under the muscular layer of the dermis. Interstitial fluids, stained in pink, can be seen throughout the implanted scaffold, in contrast to a non-implanted scaffold (Fig 1C). Within the global view it was observed that the scaffold maintains its general shape throughout the study. In Fig 3D–3F, a magnified section of the perimeter of the scaffold is shown at each post-implantation time points. At 1 week, the dermis tissue surrounding implant displays

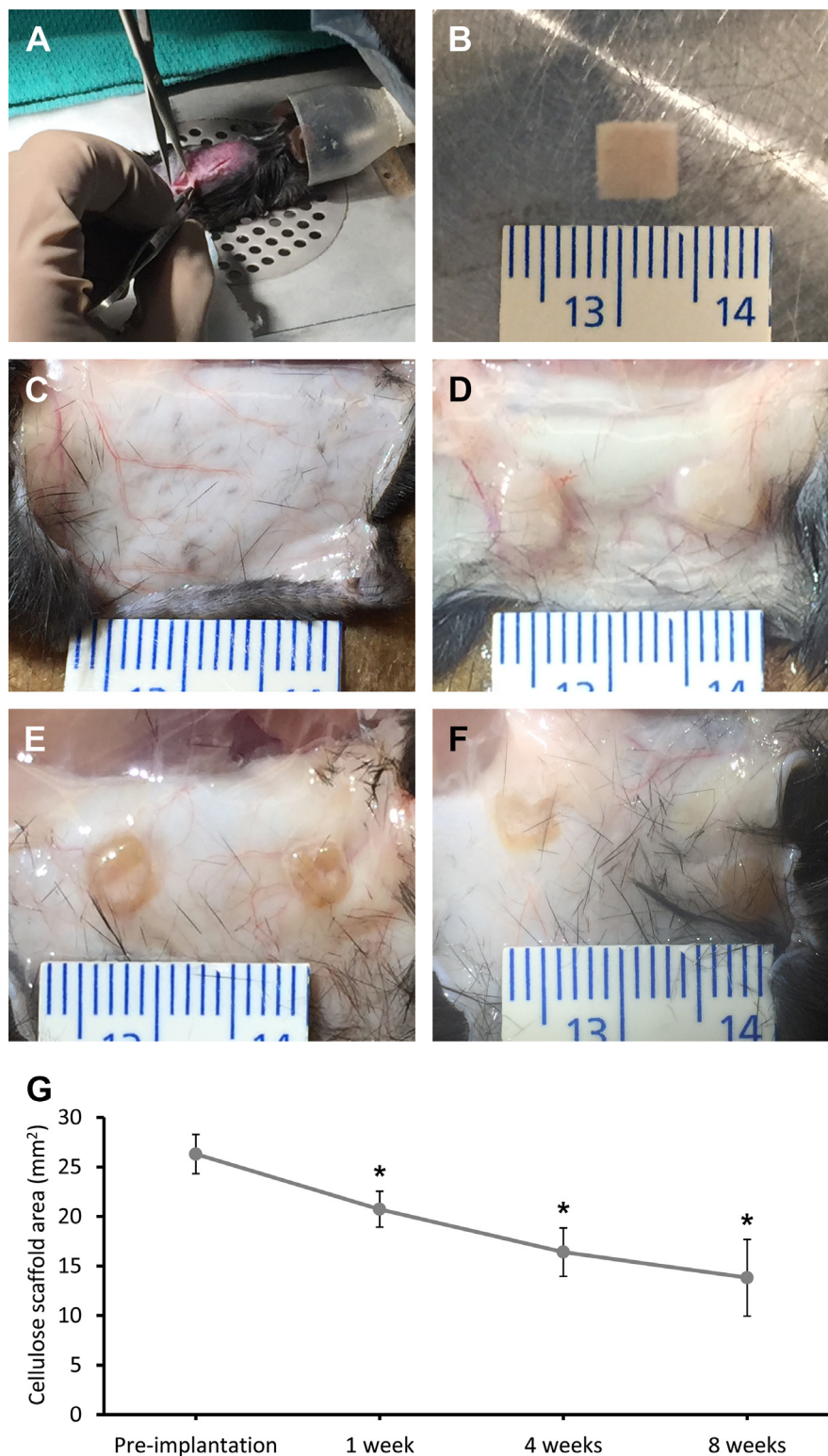


Fig 2. Cellulose scaffolds implantation and resection. The subcutaneous implantations of cellulose scaffolds biomaterial were performed on the dorsal region of a C57BL/10ScSnJ mouse model by small skin incisions (8 mm) (A). Each implant was measured before their implantation for scaffold area comparison (B). Cellulose scaffolds were resected at 1 week (D), 4 weeks (E) and 8 weeks (F) after the surgeries and macroscopic pictures were taken (control skin in C). The changes in cellulose scaffold surface area over time

are presented (G). The pre-implantation scaffold had an area of $26.30 \pm 1.98 \text{mm}^2$. Following the implantation, the area of the scaffold declined to $20.74 \pm 1.80 \text{mm}^2$ after 1 week, $16.41 \pm 2.44 \text{mm}^2$ after 4 weeks and $13.82 \pm 3.88 \text{mm}^2$ after 8 weeks. The surface area of the cellulose scaffold has a significant decrease of about 12mm^2 (48%) after 8 weeks implantation (* = $P < 0.001$; $n = 12-14$).

doi:10.1371/journal.pone.0157894.g002

symptoms of an acute moderate to severe immune response (qualitative study performed by a pathologist) (Fig 3D). As well a dense layer of cells can be seen infiltrating into the cellulose scaffolds. The population of cells within the scaffold at 1 week consist mainly of granulocytes, specifically; polymorphonuclear (PMN) and eosinophils (Fig 3D). There is also a population of dead cells and apparent cell debris. Importantly, all of these observations are completely consistent with an expected acute foreign body reaction that follows implantation [84–86]. At the 4 week point we observed a stark difference in both the surrounding epidermis and in the cell population migrating into the cellulose scaffold (Fig 3E). The epidermal tissue surrounding the cellulose scaffold has a decreased immune response, now scored as mild to low. The population of cells within the epidermis surrounding scaffolds now contain higher levels of macrophages and lymphocytes (Fig 3E). This is an anticipated characteristic of the foreign body

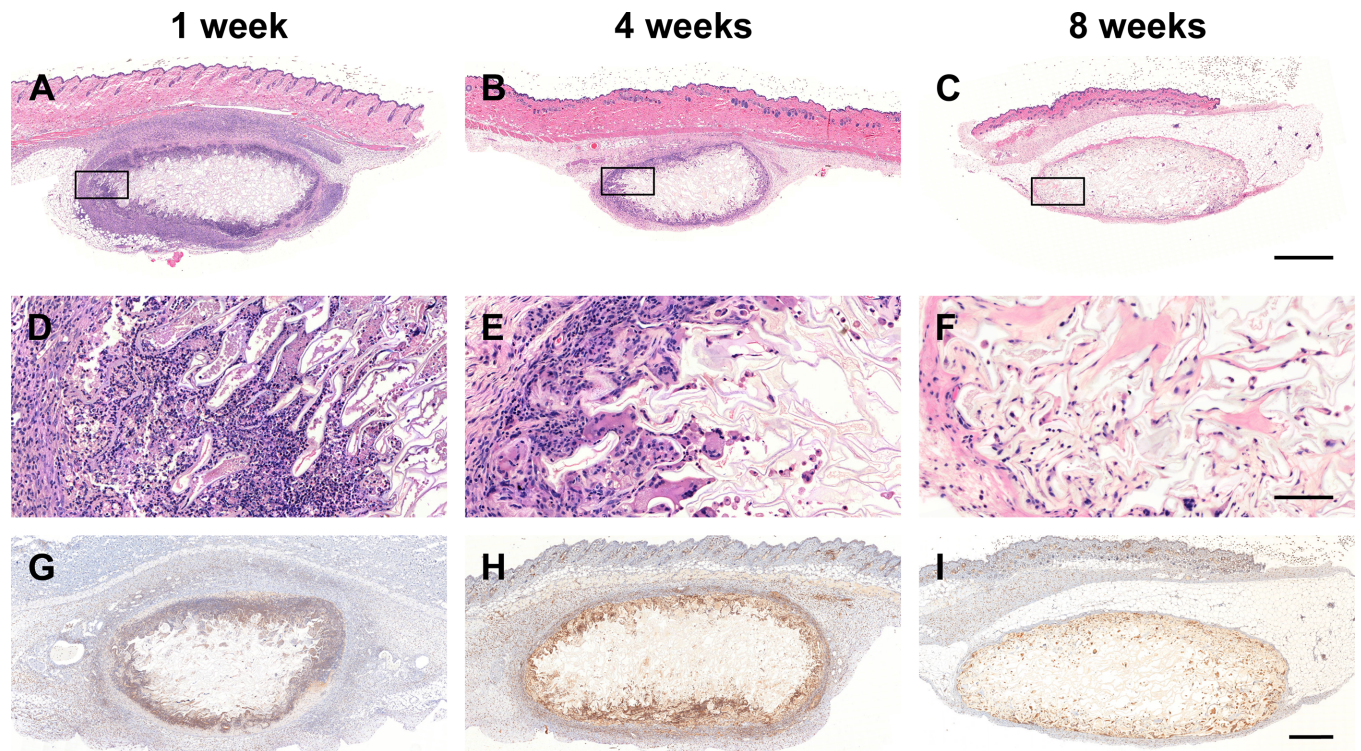


Fig 3. Biocompatibility and cell infiltration. Cross sections of representative cellulose scaffolds stained with H&E and anti-CD45. These global view show the acute moderate-severe anticipated foreign body reaction at 1 week (A), the mild chronic immune and subsequent cleaning processes at 4 weeks (B) and finally, the cellulose scaffold assimilated into the native mouse tissue at 8 weeks (C). Higher magnification regions of interest (D-F), see inset (A-C), allow the observation of all the cell type population within biomaterial assimilation processes. At 1 week, we can observe populations of granulocytes, specifically; polymorphonuclear (PMN) and eosinophils that characterize the acute moderate to severe immune response, a normal reaction to implantation procedures (D). At 4 weeks, a decreased immune response can be observed (mild to low immune response) and the population of cells within the epidermis surrounding scaffolds now contain higher levels of monocytes and lymphocytes characterizing chronic response (E). Finally, at 8 weeks, the immune response has completely resorbed with the epidermis tissue now appearing normal (F). The immune response observed with H&E staining is confirmed using anti-CD45 antibody, a well known markers of leukocytes (G-I). The population of cells within the scaffold are now mainly macrophages, multinucleated cells and active fibroblasts. Scale bars: A-C = 1mm, D-F = 100 μm and G-I = 500 μm .

doi:10.1371/journal.pone.0157894.g003

reaction to an implanted biomaterial, demonstrating the scaffold cleaning process [84–86]. There is also an increase in the population of multinucleated cells within the interior of the scaffold as part of an inflammatory response (Fig 3E). Finally, 8 weeks post-implantation, the immune response apparent at 1 and 4 weeks has completely disappeared (Fig 3F), with the epidermis tissue now appearing normal. In fact, the epidermis tissue in contact with the cellulose scaffold contains the same structures as normal epidermis tissue. In the cellulose scaffold perimeter there is now a lower density of cells due to the decreased inflammation and notably, there are no fragmented dead cells present. Instead, the population of cells now contain an elevated level of macrophages, multinucleated cells and active fibroblasts, identified through morphological analysis (H&E staining). The active fibroblasts (appearing spindle shaped), can be observed migrating from the surrounding epidermis into the cellulose scaffold. In fact, fibroblasts were found throughout the cellulose scaffold. These results demonstrate that by 8 weeks post-implantation the cellulose scaffold has been accepted by the host. In parallel with the H&E inflammation analysis, we performed anti-CD45 staining to evaluate the level of inflammation throughout the scaffold and surrounding dermis tissue (Fig 3G–3I). It is clear that the inflammation throughout the dermis and within the scaffold is elevated after 1 week. However, the amount of leukocytes significantly decreases in the surrounding dermis and scaffold over the implantation time reaching a near basal level at 8 weeks. At each time point the majority of infiltrated cells can be observed along the periphery of the cellulose scaffold. However, individual cells that have migrated from the periphery can also be observed within the center of the scaffold.

Extracellular Matrix Deposition in the Cellulose Scaffolds

The presence of active fibroblasts led us to question if the cellulose scaffold was acting as a substrate for the deposition of new extracellular matrix. This was determined using Masson's Trichrome staining of fixed cellulose scaffold slides at each time point following implantation (Fig 4). At 1-week post-implantation, the histological study shows the absence of collagen structures inside the collagen scaffold (Fig 4A, 4D and 4G). After 4-weeks, small amounts of collagen begin to be deposited inside the scaffold (Fig 4B, 4E and 4H) and by 8-weeks, large amounts of collagen are clearly visible within many scaffold cavities (Fig 4C, 4F and 4I). The presence of active fibroblasts identified through morphology (H&E staining, spindle shaped) and anti-alpha smooth muscle actin staining (data not shown) are completely consistent with the large degree of collagen deposits observed at 8-weeks. The complexity of the deposited collagen network is highlighted in Fig 4I, where individual collagen fibers within the collagen matrix are visible. This is in contrast to the characteristic high density, thick, cable-like organization of collagen found in scar tissue.

Vascularization of the Cellulose Scaffolds

Capillaries ranging from 8 to 25 μ m were also identified within the scaffolds as early as 1 week post-implantation. At 4 week and 8 week post implantation, blood vessels and capillaries can be observed extensively within the scaffold and the surrounding dermal tissue. We observed blood vessels presence on the cellulose scaffold and in surrounding dermis in the macroscopic photos taken during the resection (Fig 5A). Multiple cross sections of blood vessels, with the presence of red blood cells (RBCs), are identified within 4 weeks of scaffold implantations (Fig 5B; H&E stain). The same results are obtained 8 weeks after implantation where capillaries with RBC and endothelial cells are clearly seen (Fig 5C; Masson's Trichrome). This data prompted us to verify the presence of endothelial cells in capillary structures found within the scaffold with anti-CD31 staining (Fig 5D).

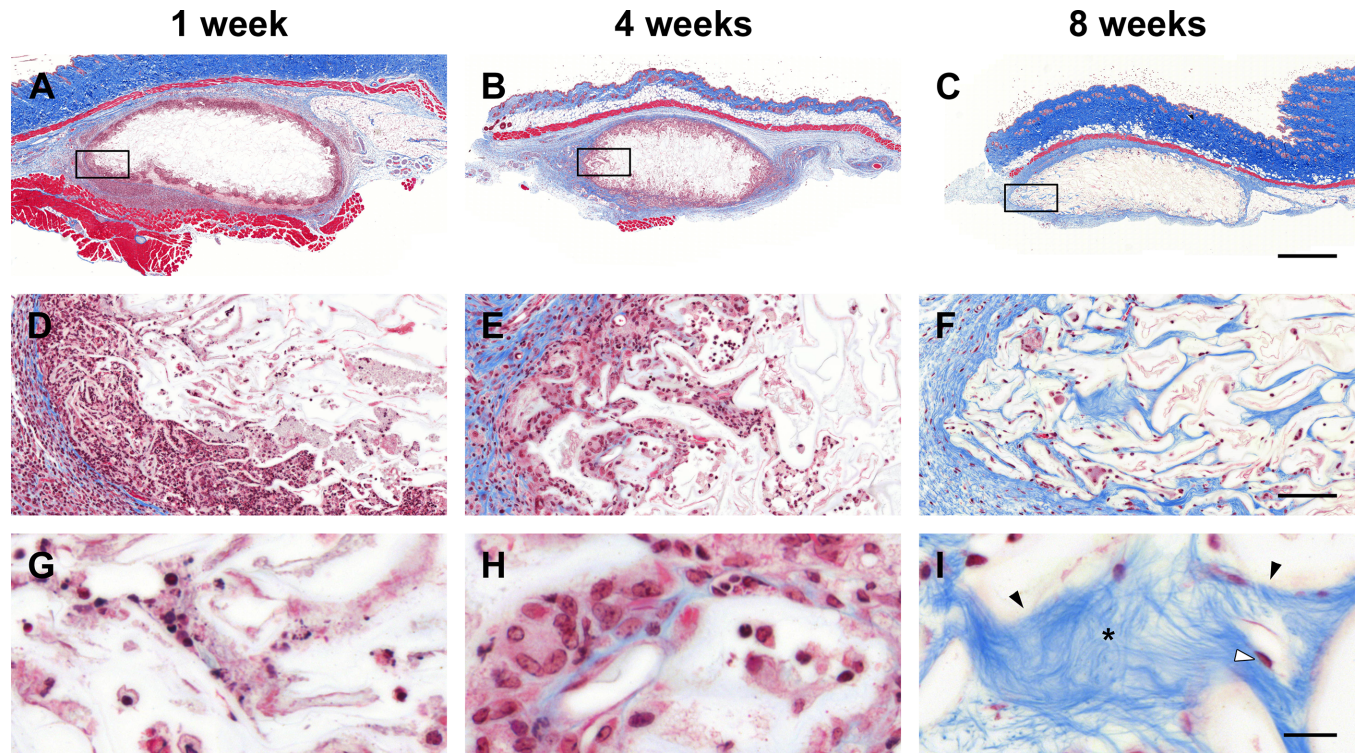


Fig 4. Extracellular matrix deposition. Cross sections of representative cellulose scaffolds stained with Masson's Trichrome (A-C). After 1 week post-implantation, the magnification of region of interest in (A), see inset, show the lack of collagen structures inside the collagen scaffold (D, G). As fibroblast cells start to invade the scaffold, collagen deposits inside the cellulose scaffold can be sparsely observed after 4 weeks (E, H). Concomitant with the observation of activated fibroblast (spindle shaped cells) inside the cellulose scaffold, collagen network is clearly visible inside the cavities after 8 weeks (F, I). Scale bars: A-C = 1mm, D-F = 100 μ m and G-I = 20 μ m. * = collagen fibers; black arrows = cellulose cell wall; white arrow = fibroblast.

doi:10.1371/journal.pone.0157894.g004

Discussion

In this study, our objective was to examine the *in vivo* biocompatibility of acellular cellulose scaffolds derived from apple hypanthium tissue. To this end, acellular cellulose scaffolds were subcutaneously implanted within immunocompetent mice to establish their biocompatibility. Our data reveals that the implanted scaffolds demonstrate a low inflammatory response, promote cell invasion and extracellular matrix deposition, and act as a pro-angiogenic environment. Remarkably, none of the mice in this study died or demonstrated any symptoms of implant rejection such as edema, exudates or discomfort during the course of this research indicative of a successful implantation of the cellulose scaffolds. The implanted scaffolds are composed of a porous network of cavities in which the original host plant cells resided [69]. This architecture efficiently facilitates transfer of nutrients throughout the plant tissue. As we have shown here and in our previous study, the apple tissues are easily decellularized [27]. This simple treatment changes the appearance of the hypanthium tissue so that it becomes transparent, as a result of the removal of cellular materials.

Several important conclusions emerge from the current study. First, after implantation, the scaffolds are rapidly infiltrated with host cells, which begin with inflammatory cells. Consistent with previous findings, the immune response of the host animals followed a well-known timeline [84–88], ultimately demonstrating biocompatibility. As expected, the cell population within the scaffold after 1 week post-implantation are mainly granulocytes, specifically; polymorphonuclear (PMN) and eosinophils, constituting a clear inflammatory response. The

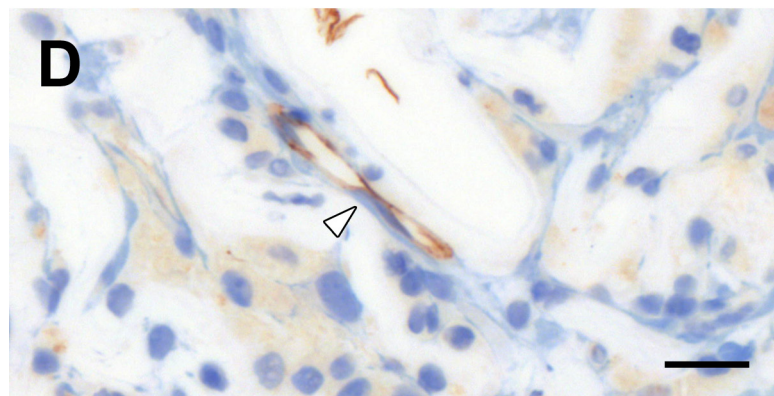
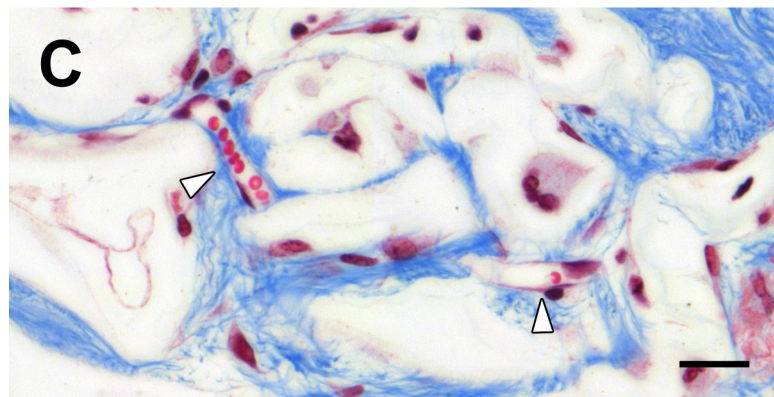
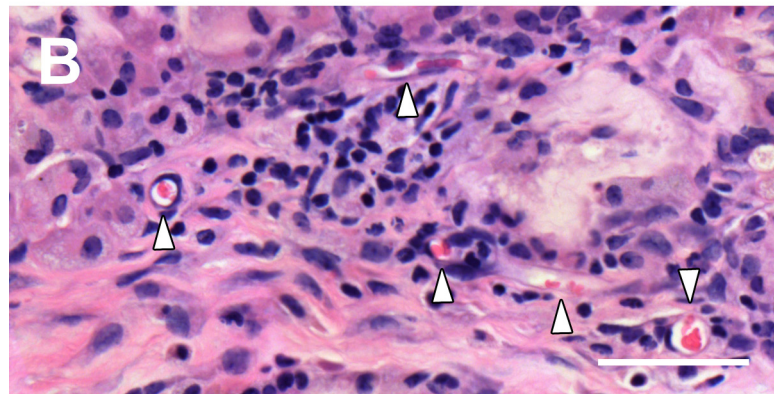
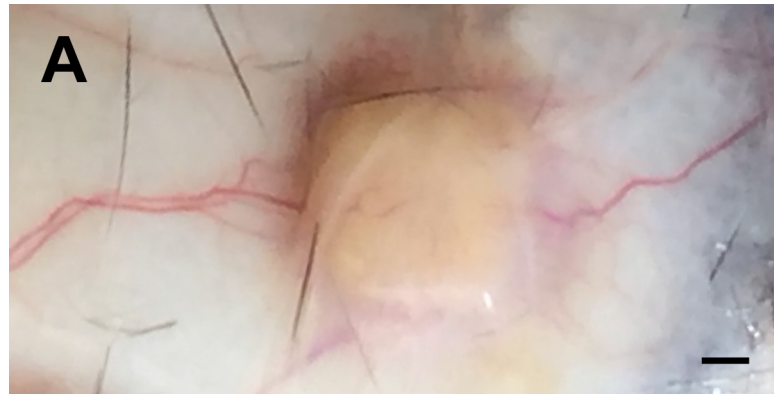


Fig 5. Vascularization and Angiogenesis. Macroscopic observations of blood vessels directly in the surrounding tissues around the cellulose scaffold (A). Confirmation of angiogenesis within the cellulose scaffold by the observation of multiple blood vessel cross sections in H&E staining (B) and Masson's Trichrome staining (C) micrographs. The angiogenesis process was also confirmed with anti-CD31 staining to identify endothelial cells within the cellulose scaffold (D). Scale bars: A = 1mm, B = 50 μ m and C-D = 20 μ m. White arrows = blood vessels.

doi:10.1371/journal.pone.0157894.g005

production of a provisional matrix around the scaffold was also observed resulting in an inflamed appearance in the tissue surrounding the scaffold [84–88]. This is not unexpected and is the result of the foreign material as well as a response to the surgical procedure [84–88]. Four weeks post implantation, the population of cells within the scaffold have evolved and are now lymphocytes, monocytes, macrophages, foreign body multinucleated cells as well as scattered eosinophils. Typical with chronic inflammation, the cellular debris present in the provisional matrix at 1 week, is now being cleared by the host immune system [84–88]. At 8 weeks, the cellulose scaffold is now void of all provisional matrix and cellular debris and low levels of macrophages and foreign body multinucleated cells are still visible within the scaffold. Consistent with the immune response within the cellulose scaffold, the surrounding tissue is observed to return to its original physiology. In fact, at 8 week implantation the surrounding tissue is nearly similar to control tissue. Although the immune response and inflammation at 8 weeks is low, low levels of macrophages can be observed within the scaffold. Although traditionally associated with inflammation, macrophages have beneficial roles consistent with our findings. Specifically, macrophages are also known to secrete growth and pro-angiogenic factors, ECM proteins and pro-fibrogenic factors that actively regulate the fibro-proliferation and angiogenesis in tissue repair and regeneration [86]. Regardless, the vast population of cells within the scaffold after 8 weeks are now reactive fibroblasts. These cells are altering the microenvironment of the scaffold through the secretion of a new collagen extracellular matrix. Importantly the new matrix displays a remarkably low density compared, suggestive of regeneration as opposed to the characteristic high density, cable-like organization of collagen found in scar tissues [89]. In the Fig 3D–3F, the majority of cells can be observed infiltrating primarily along the periphery of the cellulose scaffold. As the cellulose scaffold is composed of interconnecting cell wall cavities it is expected that it would be more difficult to migrate into the central portion of the scaffold. Limited cell infiltration is an issue with all novel biomaterials and as such researchers are constantly modifying the physical and chemical properties of established biomaterials to enhance the cell infiltration [90–92]. Now that we have confirmed the biocompatibility of the scaffold, in future studies we will be systematically modify the structure and mechanics of the scaffolds to enable optimal cell infiltration.

Our data also demonstrates that the scaffolds are pro-angiogenic, which is critical to ensuring blood transport from the surrounding tissue [93]. As with native tissue, limited blood supply to the scaffold will result in ischemia and potentially necrosis. Interestingly, it was demonstrated that bioceramics with small pore diameters limits blood vessel diameter *in vivo*. The porous structure of the cellulose scaffolds is due to overlapping cavities with an average internal cross-sectional area of $0.013 \pm 0.007 \text{mm}^2$ (as determined from H&E images). There was a large distribution in the size of the cavities with diameters ranging from 100–300 μ m with minimal interconnection distance of $4.04 \pm 1.4 \mu\text{m}$. As such, the low cell wall fiber volume-fraction of $16.9 \pm 3.07\%$ of the cellulose scaffolds are consistent with the promotion of blood vessel formation [94]. At 4 and 8 week implantation time we observed blood vessels formation within the cellulose scaffold. Interestingly, blood vessel formation are apparent in various biomaterials at similar implantation times [95,96]. Taken together, the cellulose scaffold now appears to completely void of the provisional matrix and fully accepted as a subcutaneous implant.

We also observed a decrease in the scaffold area over time, but it does not appear that the cellulose scaffold is in the processes of degradation. Rather, the change in area is due to the collapse of the cell wall cavities on the perimeter of the scaffold resulting from the active movement of the mouse. Active biological degradation is not expected to be possible as mammals lack the appropriate enzymes to digest plant-synthesized cellulose [97,98]. Moreover, the highly crystalline form of cellulose that is found in plant tissues is also known to be resistant to degradation in mammals [98]. Alternatively, it has been demonstrated that *in vivo* cellulose based implants can be chemically activated in order to be more easily degraded [99]. Most importantly however, highly crystalline forms of cellulose have some of the lowest reported immunological responses [98].

A large variety of clinically approved biomaterials are used to treat specific conditions within patients [1]. Such biomaterials can be derived from human and animal tissues, synthetic polymers, as well as materials such as titanium and ceramics [1,2,26,49,50,53,54,56,74,76,94,96,100–110]. However, these approaches are not without disadvantages that arise from concerns about the source, production costs and/or widespread availability [48]. There is currently an intense interest in developing resorbable biomaterials that will degrade *in vivo* and only act as a temporary scaffold that will promote and support the repair or regeneration of damaged/diseased tissue [49]. Although this is an ideal scenario, newly formed structures are also found to collapse as the scaffold degrades [53,64,111–113]. Moreover, the products of degradation can also be found to have toxic or undesirable side-effects [53,114,115]. For example, the reconstruction of the ear has become a well-known challenge in tissue engineering. Early studies have employed scaffolds in the shape of an ear that are produced from animal or human derived cartilage [53,58,59,61,63,64]. However, after implantation and eventual scaffold degradation, the ear is often found to collapse or deform [60–62]. Recent strategies have now opted to create biological composite materials composed of both a titanium frame embedded in a biological matrix [53]. Therefore, there is still a clear need for non-resorbable, yet inert and biocompatible, scaffolds persists in the field of tissue and organ engineering.

We suggest that plant-derived cellulose biomaterials offer one potential approach for the production of implantable scaffolds. This approach is complementary to bacterial cellulose strategies which have demonstrated clear utility as well [66,69–71,73,80,83,108,110,116–119]. However, plant derived materials are cost effective to produce and are extremely straightforward to prepare for implantation, exhibit clear biocompatibility, an ability to retain their shape while supporting the production of natural extracellular matrix and most importantly, the promotion of vascularization. In our previous work we have shown that the scaffolds can also be functionalized with proteins prior to culture *in vitro*. Such work will also be conducted in the future in order to explore the use of scaffold surface functionalization with growth factors and matrix proteins to promote the invasion of specific cell types, further minimize the early immune response and promote maximal vascularization. Moreover, the cellulose scaffolds can easily be formed into specific shapes and sizes, offering an opportunity to create new tissues with specific geometrical properties. Although there are numerous new avenues of research to follow, we have been able to demonstrate that acellular cellulose scaffolds are biocompatible *in vivo* in immunocompetent mice and might be considered as a new strategy for tissue regeneration.

Acknowledgments

We thank Joshua Lavigne, VT, RLAT for technical assistance with animals, Ana Giassi, PhD for histological processing and Manijeh Daneshmand, MD for her histopathological analysis. We thank Virgile Koffi and Nathan Adolphe for pictures in [Fig 1A and 1B](#).

Author Contributions

Conceived and designed the experiments: DJM CMC AEP. Performed the experiments: DJM CMC AEP. Analyzed the data: DJM CMC AEP. Contributed reagents/materials/analysis tools: DJM CMC AEP. Wrote the paper: DJM CMC AEP.

References

1. Saini M. Implant biomaterials: A comprehensive review. *World J Clin Cases*. 2015; 3: 52. doi: [10.12998/wjcc.v3.i1.52](https://doi.org/10.12998/wjcc.v3.i1.52) PMID: [25610850](https://pubmed.ncbi.nlm.nih.gov/25610850/)
2. Pashuck ET, Stevens MM. STATE OF THE ART REVIEW Designing Regenerative Biomaterial Therapies for the Clinic. *Sci Transl Med*. 2012; 4.
3. Athanasiou KA, Reddi AH, Gulberg RE, Revell CM. Special section. 2012;338: 921–927.
4. Kar M, Vernon Shih Y-R, Velez DO, Cabrales P, Varghese S. Poly(ethylene glycol) hydrogels with cell cleavable groups for autonomous cell delivery. *Biomaterials*. 2016; 77: 186–97. doi: [10.1016/j.biomaterials.2015.11.018](https://doi.org/10.1016/j.biomaterials.2015.11.018) PMID: [26606444](https://pubmed.ncbi.nlm.nih.gov/26606444/)
5. Gu L, Mooney DJ. Biomaterials and emerging anticancer therapeutics: engineering the microenvironment. *Nat Rev Cancer*. Nature Publishing Group, a division of Macmillan Publishers Limited. All Rights Reserved.; 2015; 16: 56–66. doi: [10.1038/nrc.2015.3](https://doi.org/10.1038/nrc.2015.3)
6. Maurer M, Röhrnbauer B, Feola A, Deprest J, Mazza E. Prosthetic Meshes for Repair of Hernia and Pelvic Organ Prolapse: Comparison of Biomechanical Properties. *Materials (Basel)*. Multidisciplinary Digital Publishing Institute; 2015; 8: 2794–2808. doi: [10.3390/ma8052794](https://doi.org/10.3390/ma8052794)
7. Mao AS, Mooney DJ. Regenerative medicine: Current therapies and future directions. *Proc Natl Acad Sci*. 2015; 112: 201508520. doi: [10.1073/pnas.1508520112](https://doi.org/10.1073/pnas.1508520112)
8. Hsu S-H, Hsieh P-S. Self-assembled adult adipose-derived stem cell spheroids combined with biomaterials promote wound healing in a rat skin repair model. *Wound Repair Regen*. 23: 57–64. doi: [10.1111/wrr.12239](https://doi.org/10.1111/wrr.12239) PMID: [25421559](https://pubmed.ncbi.nlm.nih.gov/25421559/)
9. Guillaume O, Park J, Monforte X, Gruber-Blum S, Redl H, Petter-Puchner A, et al. Fabrication of silk mesh with enhanced cytocompatibility: preliminary *in vitro* investigation toward cell-based therapy for hernia repair. *J Mater Sci Mater Med*. 2016; 27: 37. doi: [10.1007/s10856-015-5648-3](https://doi.org/10.1007/s10856-015-5648-3) PMID: [26704554](https://pubmed.ncbi.nlm.nih.gov/26704554/)
10. Soto-Gutierrez A, Zhang L, Medberry C, Fukumitsu K, Faulk D, Jiang H, et al. A whole-organ regenerative medicine approach for liver replacement. *Tissue Eng Part C Methods*. Mary Ann Liebert, Inc. 140 Huguenot Street, 3rd Floor New Rochelle, NY 10801 USA; 2011; 17: 677–86. doi: [10.1089/ten.TEC.2010.0698](https://doi.org/10.1089/ten.TEC.2010.0698) PMID: [21375407](https://pubmed.ncbi.nlm.nih.gov/21375407/)
11. Badylak SF, Taylor D, Uygun K. Whole-Organ Tissue Engineering: Decellularization and Recellularization of Three-Dimensional Matrix Scaffolds. *Annual Reviews*; 2011; Available: <http://www.annualreviews.org/doi/abs/10.1146/annurev-bioeng-071910-124743>
12. Baptista PM, Orlando G, Mirmalek-Sani S-H, Siddiqui M, Atala A, Soker S. Whole organ decellularization—a tool for bioscaffold fabrication and organ bioengineering. *Conf Proc. Annu Int Conf IEEE Eng Med Biol Soc IEEE Eng Med Biol Soc Annu Conf*. 2009; 2009: 6526–9. doi: [10.1109/IEMBS.2009.5333145](https://doi.org/10.1109/IEMBS.2009.5333145)
13. Baptista PM, Siddiqui MM, Lozier G, Rodriguez SR, Atala A, Soker S. The use of whole organ decellularization for the generation of a vascularized liver organoid. *Hepatology*. 2011; 53: 604–617. doi: [10.1002/hep.24067](https://doi.org/10.1002/hep.24067) PMID: [21274881](https://pubmed.ncbi.nlm.nih.gov/21274881/)
14. Ott HC, Matthiesen TS, Goh SK, Black LD, Kren SM, Netoff TI, et al. Perfusion-decellularized matrix: using nature's platform to engineer a bioartificial heart. *Nat Med*. 2008; 14: 213–21. doi: [10.1038/nm1684](https://doi.org/10.1038/nm1684) PMID: [18193059](https://pubmed.ncbi.nlm.nih.gov/18193059/)
15. Song JJ, Ott HC. Organ engineering based on decellularized matrix scaffolds. *Trends Mol Med*. Elsevier Ltd; 2011; 17: 424–32. doi: [10.1016/j.molmed.2011.03.005](https://doi.org/10.1016/j.molmed.2011.03.005) PMID: [21514224](https://pubmed.ncbi.nlm.nih.gov/21514224/)
16. Badylak SF. The extracellular matrix as a biologic scaffold material. *Biomaterials*. 2007; 28: 3587–3593. doi: [10.1016/j.biomaterials.2007.04.043](https://doi.org/10.1016/j.biomaterials.2007.04.043) PMID: [17524477](https://pubmed.ncbi.nlm.nih.gov/17524477/)
17. Lv S, Dudek DM, Cao Y, Balamurali MM, Gosline J, Li H. Designed biomaterials to mimic the mechanical properties of muscles. *Nature*. 2010; 465: 69–73. doi: [10.1038/nature09024](https://doi.org/10.1038/nature09024) PMID: [20445626](https://pubmed.ncbi.nlm.nih.gov/20445626/)
18. Campoli G, Borleffs MS, Amin Yavari S, Wauthle R, Weinans H, Zadpoor a. a. Mechanical properties of open-cell metallic biomaterials manufactured using additive manufacturing. *Mater Des*. 2013; 49: 957–965. doi: [10.1016/j.matdes.2013.01.071](https://doi.org/10.1016/j.matdes.2013.01.071)

19. Anseth KS, Bowman CN, Brannon-Peppas L. Mechanical properties of hydrogels and their experimental determination. *Biomaterials*. 1996; 17: 1647–1657. doi: [10.1016/0142-9612\(96\)87644-7](https://doi.org/10.1016/0142-9612(96)87644-7) PMID: [8866026](https://pubmed.ncbi.nlm.nih.gov/8866026/)
20. Zhao R, Sider KL, Simmons C a. Measurement of layer-specific mechanical properties in multilayered biomaterials by micropipette aspiration. *Acta Biomater*. 2011; 7: 1220–1227. doi: [10.1016/j.actbio.2010.11.004](https://doi.org/10.1016/j.actbio.2010.11.004) PMID: [21056128](https://pubmed.ncbi.nlm.nih.gov/21056128/)
21. Chen Q, Liang S, Thouas G a. Elastomeric biomaterials for tissue engineering. *Prog Polym Sci*. 2013; 38: 584–671. doi: [10.1016/j.progpolymsci.2012.05.003](https://doi.org/10.1016/j.progpolymsci.2012.05.003)
22. Guzman RC de, Merrill MR, Richter JR, Hamzi RI, Greengauz-Roberts OK, Van Dyke ME. Mechanical and biological properties of keratose biomaterials. *Biomaterials*. 2011; 32: 8205–17. doi: [10.1016/j.biomaterials.2011.07.054](https://doi.org/10.1016/j.biomaterials.2011.07.054) PMID: [21835462](https://pubmed.ncbi.nlm.nih.gov/21835462/)
23. Staiger MP, Pietak AM, Huadmai J, Dias G. Magnesium and its alloys as orthopedic biomaterials: A review. *Biomaterials*. 2006; 27: 1728–1734. doi: [10.1016/j.biomaterials.2005.10.003](https://doi.org/10.1016/j.biomaterials.2005.10.003) PMID: [16246414](https://pubmed.ncbi.nlm.nih.gov/16246414/)
24. Bagno A, Di Bello C. Surface treatments and roughness properties of Ti-based biomaterials. *J Mater Sci Mater Med*. 2004; 15: 935–49. doi: [10.1023/B:JMSM.0000042679.28493.7f](https://doi.org/10.1023/B:JMSM.0000042679.28493.7f) PMID: [15448401](https://pubmed.ncbi.nlm.nih.gov/15448401/)
25. Tibbitt MW, Anseth KS. Dynamic Microenvironments: The Fourth Dimension. 2012; 4: 1–5.
26. Lemons JE, Lucas LC. Properties of biomaterials. *J Arthroplasty*. 1986; 1: 143–147. doi: [10.1016/S0883-5403\(86\)80053-5](https://doi.org/10.1016/S0883-5403(86)80053-5) PMID: [3559583](https://pubmed.ncbi.nlm.nih.gov/3559583/)
27. Modulevsky DJ, Lefebvre C, Haase K, Al-Rekabi Z, Pelling AE. Apple Derived Cellulose Scaffolds for 3D Mammalian Cell Culture. Kerkis I, editor. *PLoS One*. 2014; 9: e97835. doi: [10.1371/journal.pone.0097835](https://doi.org/10.1371/journal.pone.0097835) PMID: [24842603](https://pubmed.ncbi.nlm.nih.gov/24842603/)
28. Tibbitt MW, Anseth KS. Hydrogels as extracellular matrix mimics for 3D cell culture. *Biotechnol Bioeng*. 2009; 103: 655–63. doi: [10.1002/bit.22361](https://doi.org/10.1002/bit.22361) PMID: [19472329](https://pubmed.ncbi.nlm.nih.gov/19472329/)
29. Vacanti JP, Lal B, Grad O, Darling EM, Hu JC, Wiesmann HP, et al. Special section. 2012;338: 921–926.
30. Why Organ, Eye and Tissue Donation? In: U.S. Department of Health and Human Services [Internet]. Available: <http://www.organdonor.gov/index.html>
31. Sterling JA, Guelcher SA. Biomaterial scaffolds for treating osteoporotic bone. *Curr Osteoporos Rep*. 2014; 12: 48–54. doi: [10.1007/s11914-014-0187-2](https://doi.org/10.1007/s11914-014-0187-2) PMID: [24458428](https://pubmed.ncbi.nlm.nih.gov/24458428/)
32. Abou Neel EA, Chrzanowski W, Salih VM, Kim H-W, Knowles JC. Tissue engineering in dentistry. *J Dent*. 2014; 42: 915–28. doi: [10.1016/j.jdent.2014.05.008](https://doi.org/10.1016/j.jdent.2014.05.008) PMID: [24880036](https://pubmed.ncbi.nlm.nih.gov/24880036/)
33. Shue L, Yufeng Z, Mony U. Biomaterials for periodontal regeneration: a review of ceramics and polymers. *Biomatter*. 2: 271–7. doi: [10.4161/biom.22948](https://doi.org/10.4161/biom.22948) PMID: [23507891](https://pubmed.ncbi.nlm.nih.gov/23507891/)
34. O'Brien FJ. Biomaterials & scaffolds for tissue engineering. *Mater Today*. 2011; 14: 88–95. doi: [10.1016/S1369-7021\(11\)70058-X](https://doi.org/10.1016/S1369-7021(11)70058-X)
35. Bhardwaj N, Devi D, Mandal BB. Tissue-engineered cartilage: the crossroads of biomaterials, cells and stimulating factors. *Macromol Biosci*. 2015; 15: 153–82. doi: [10.1002/mabi.201400335](https://doi.org/10.1002/mabi.201400335) PMID: [25283763](https://pubmed.ncbi.nlm.nih.gov/25283763/)
36. Metcalfe AD, Ferguson MWJ. Tissue engineering of replacement skin: the crossroads of biomaterials, wound healing, embryonic development, stem cells and regeneration. *J R Soc Interface*. 2007; 4: 413–37. doi: [10.1098/rsif.2006.0179](https://doi.org/10.1098/rsif.2006.0179) PMID: [17251138](https://pubmed.ncbi.nlm.nih.gov/17251138/)
37. Takebe T, Sekine K, Enomura M, Koike H, Kimura M, Ogaeri T, et al. Vascularized and functional human liver from an iPSC-derived organ bud transplant. *Nature*. Nature Publishing Group, a division of Macmillan Publishers Limited. All Rights Reserved.; 2013; 499: 481–4. doi: [10.1038/nature12271](https://doi.org/10.1038/nature12271) PMID: [23823721](https://pubmed.ncbi.nlm.nih.gov/23823721/)
38. Mannoor MS, Jiang Z, James T, Kong YL, Malatesta KA, Soboyejo WO, et al. 3D printed bionic ears. *Nano Lett*. American Chemical Society; 2013; 13: 2634–9. doi: [10.1021/nl4007744](https://doi.org/10.1021/nl4007744) PMID: [23635097](https://pubmed.ncbi.nlm.nih.gov/23635097/)
39. Raya-Rivera AM, Esquiliano D, Fierro-Pastrana R, López-Bayghen E, Valencia P, Ordorica-Flores R, et al. Tissue-engineered autologous vaginal organs in patients: a pilot cohort study. *Lancet (London, England)*. Elsevier; 2014; 384: 329–36. doi: [10.1016/S0140-6736\(14\)60542-0](https://doi.org/10.1016/S0140-6736(14)60542-0)
40. Salzberg CA. Nonexpansive immediate breast reconstruction using human acellular tissue matrix graft (AlloDerm). *Ann Plast Surg*. 2006; 57: 1–5. doi: [10.1097/01.sap.0000214873.13102.9f](https://doi.org/10.1097/01.sap.0000214873.13102.9f) PMID: [16799299](https://pubmed.ncbi.nlm.nih.gov/16799299/)
41. Lee DK. Achilles Tendon Repair with Acellular Tissue Graft Augmentation in Neglected Ruptures. *J Foot Ankle Surg*. 2007; 46: 451–455. doi: [10.1053/j.jfas.2007.05.007](https://doi.org/10.1053/j.jfas.2007.05.007) PMID: [17980842](https://pubmed.ncbi.nlm.nih.gov/17980842/)
42. Cornwell KG, Landsman A, James KS. Extracellular Matrix Biomaterials for Soft Tissue Repair. *Clin Podiatr Med Surg*. 2009; 26: 507–523. doi: [10.1016/j.cpm.2009.08.001](https://doi.org/10.1016/j.cpm.2009.08.001) PMID: [19778685](https://pubmed.ncbi.nlm.nih.gov/19778685/)

43. Ren X, Moser PT, Gilpin SE, Okamoto T, Wu T, Tapias LF, et al. Engineering pulmonary vasculature in decellularized rat and human lungs. *Nat Biotechnol.* 2015; 33: 1097–102. doi: [10.1038/nbt.3354](https://doi.org/10.1038/nbt.3354) PMID: [26368048](https://pubmed.ncbi.nlm.nih.gov/26368048/)
44. Guyette JP, Charest J, Mills RW, Jank B, Moser PT, Gilpin SE, et al. Bioengineering Human Myocardium on Native Extracellular Matrix. *Circ Res.* 2015; CIRCRESAHA.115.306874–. doi: [10.1161/CIRCRESAHA.115.306874](https://doi.org/10.1161/CIRCRESAHA.115.306874)
45. Raya-Rivera A, Esquiliano DR, Yoo JJ, Lopez-Bayghen E, Soker S, Atala A. Tissue-engineered autologous urethras for patients who need reconstruction: an observational study. *Lancet (London, England).* 2011; 377: 1175–82. doi: [10.1016/S0140-6736\(10\)62354-9](https://doi.org/10.1016/S0140-6736(10)62354-9)
46. Atala A, Bauer SB, Soker S, Yoo JJ, Retik AB. Tissue-engineered autologous bladders for patients needing cystoplasty. *Lancet.* 2006; 367: 1241–6. doi: [10.1016/S0140-6736\(06\)68438-9](https://doi.org/10.1016/S0140-6736(06)68438-9) PMID: [16631879](https://pubmed.ncbi.nlm.nih.gov/16631879/)
47. Hattori N. Cerebral organoids model human brain development and microcephaly. *Mov Disord.* Nature Publishing Group; 2014; 29: 185–185. doi: [10.1002/mds.25740](https://doi.org/10.1002/mds.25740) PMID: [24375826](https://pubmed.ncbi.nlm.nih.gov/24375826/)
48. Gottenbos B, Busscher HJ, Van Der Mei HC, Nieuwenhuis P. Pathogenesis and prevention of biomaterial centered infections. *J Mater Sci Mater Med.* 2002; 13: 717–722. doi: [10.1023/A:1016175502756](https://doi.org/10.1023/A:1016175502756) PMID: [15348557](https://pubmed.ncbi.nlm.nih.gov/15348557/)
49. Bohner M. Resorbable biomaterials as bone graft substitutes. *Mater Today.* 2010; 13: 24–30. doi: [10.1016/S1369-7021\(10\)70014-6](https://doi.org/10.1016/S1369-7021(10)70014-6)
50. Ratner BD, Hoffman AS, Schoen FJ, Lemons JE. Biomaterials science: an introduction to materials in medicine. *Chemical Engineering.* 2004.
51. Bae H, Puranik AS, Gauvin R, Edalat F, Peppas NA, Khademhosseini A. Building Vascular Networks. 2012; 4: 1–6.
52. Dong W, Hou L, Li T, Gong Z, Huang H, Wang G, et al. A Dual Role of Graphene Oxide Sheet Deposition on Titanate Nanowire Scaffolds for Osteo-implantation: Mechanical Hardener and Surface Activity Regulator. *Sci Rep.* Nature Publishing Group; 2015; 5: 18266. doi: [10.1038/srep18266](https://doi.org/10.1038/srep18266) PMID: [26687002](https://pubmed.ncbi.nlm.nih.gov/26687002/)
53. Zhou L, Pomerantseva I, Bassett EK, Bowley CM, Zhao X, Bichara D a, et al. Engineering ear constructs with a composite scaffold to maintain dimensions. *Tissue Eng Part A.* 2011; 17: 1573–1581. doi: [10.1089/ten.tea.2010.0627](https://doi.org/10.1089/ten.tea.2010.0627) PMID: [21284558](https://pubmed.ncbi.nlm.nih.gov/21284558/)
54. Temenoff JS, Mikos AG. Injectable biodegradable materials for orthopedic tissue engineering. *Biomaterials.* 2000; 21: 2405–2412. doi: [10.1016/S0142-9612\(00\)00108-3](https://doi.org/10.1016/S0142-9612(00)00108-3) PMID: [11055288](https://pubmed.ncbi.nlm.nih.gov/11055288/)
55. Comprehensive Biomaterials: Online Version, Volume 1 [Internet]. Newnes; 2011. Available: <https://books.google.com/books?id=oa8YpRsD1kkC&pgis=1>
56. Bao G, Suresh S. Cell and molecular mechanics of biological materials. *Nat Mater.* 2003; 2: 715–25. doi: [10.1038/nmat1001](https://doi.org/10.1038/nmat1001) PMID: [14593396](https://pubmed.ncbi.nlm.nih.gov/14593396/)
57. Place ES, Evans ND, Stevens MM. Complexity in biomaterials for tissue engineering. *Nat Mater.* Nature Publishing Group; 2009; 8: 457–470. doi: [10.1038/nmat2441](https://doi.org/10.1038/nmat2441) PMID: [19458646](https://pubmed.ncbi.nlm.nih.gov/19458646/)
58. Pomerantseva I, Bichara DA, Tseng A, Cronce MJ, Cervantes TM, Kimura AM, et al. Ear-Shaped Stable Auricular Cartilage Engineered from Extensively Expanded Chondrocytes in an Immunocompetent Experimental Animal Model. *Tissue Eng Part A.* 2015;00: ten.tea.2015.0173. doi: [10.1089/ten.tea.2015.0173](https://doi.org/10.1089/ten.tea.2015.0173)
59. Xu J-W, Johnson TS, Motarjem PM, Peretti GM, Randolph MA, Yaremchuk MJ. Tissue-engineered flexible ear-shaped cartilage. *Plast Reconstr Surg.* 2005; 115: 1633–41. Available: <http://www.ncbi.nlm.nih.gov/pubmed/15861068> PMID: [15861068](https://pubmed.ncbi.nlm.nih.gov/15861068/)
60. Shieh S-J, Terada S, Vacanti JP. Tissue engineering auricular reconstruction: *in vitro* and *in vivo* studies. *Biomaterials.* 2004; 25: 1545–57. Available: <http://www.ncbi.nlm.nih.gov/pubmed/14697857> PMID: [14697857](https://pubmed.ncbi.nlm.nih.gov/14697857/)
61. Neumeister MW, Wu T, Chambers C. Vascularized tissue-engineered ears. *Plast Reconstr Surg.* 2006; 117: 116–22. Available: <http://www.ncbi.nlm.nih.gov/pubmed/16404257> PMID: [16404257](https://pubmed.ncbi.nlm.nih.gov/16404257/)
62. Isogai N, Asamura S, Higashi T, Ikada Y, Morita S, Hillyer J, et al. Tissue engineering of an auricular cartilage model utilizing cultured chondrocyte-poly(L-lactide-epsilon-caprolactone) scaffolds. *Tissue Eng.* 10: 673–87. doi: [10.1089/1076327041348527](https://doi.org/10.1089/1076327041348527) PMID: [15265285](https://pubmed.ncbi.nlm.nih.gov/15265285/)
63. Cervantes TM, Bassett EK, Tseng A, Kimura A, Roscioli N, Randolph M a, et al. Design of composite scaffolds and three-dimensional shape analysis for tissue-engineered ear. *J R Soc Interface.* 2013; 10: 20130413. doi: [10.1098/rsif.2013.0413](https://doi.org/10.1098/rsif.2013.0413) PMID: [23904585](https://pubmed.ncbi.nlm.nih.gov/23904585/)
64. Liao HT, Zheng R, Liu W, Zhang WJ, Cao Y, Zhou G. Prefabricated, Ear-Shaped Cartilage Tissue Engineering by Scaffold-Free Porcine Chondrocyte Membrane. *Plast Reconstr Surg.* 2015; 135: 313–321. doi: [10.1097/PRS.0000000000001105](https://doi.org/10.1097/PRS.0000000000001105)

65. Lee J-S. 3D printing of composite tissue with complex shape applied to ear regeneration. *Biofabrication*. 2014; 6. Available: http://resolver.scholarsportal.info/resolve/17585082/v06i0002/024103_3pocwcsater.xml
66. Pértile RAN, Moreira S, Gil RM, Correia A, Guãrdao L. Bacterial Cellulose: Long-Term Biocompatibility Studies. *J Biomater Sci Polym Ed*. 2012; 23: 1339–1354. doi: [10.1163/092050611X581516](https://doi.org/10.1163/092050611X581516) PMID: [21722421](https://pubmed.ncbi.nlm.nih.gov/21722421/)
67. Entcheva E, Bien H, Yin L, Chung CY, Farrell M, Kostov Y. Functional cardiac cell constructs on cellulose-based scaffolding. *Biomaterials*. 2004; 25: 5753–62. doi: [10.1016/j.biomaterials.2004.01.024](https://doi.org/10.1016/j.biomaterials.2004.01.024) PMID: [15147821](https://pubmed.ncbi.nlm.nih.gov/15147821/)
68. Ishihara K, Miyazaki H, Kurosaki T, Nakabayashi N. Improvement of blood compatibility on cellulose dialysis membrane. 111. Synthesis and performance of water-soluble cellulose grafted with phospholipid polymer as coating material on cellulose dialysis membrane. *J Biomed Mater Res*. 1995; 29: 181–188. PMID: [7738064](https://pubmed.ncbi.nlm.nih.gov/7738064/)
69. Bäckdahl H, Helenius G, Bodin A, Nannmark U, Johansson BR, Risberg B, et al. Mechanical properties of bacterial cellulose and interactions with smooth muscle cells. *Biomaterials*. 2006; 27: 2141–9. doi: [10.1016/j.biomaterials.2005.10.026](https://doi.org/10.1016/j.biomaterials.2005.10.026) PMID: [16310848](https://pubmed.ncbi.nlm.nih.gov/16310848/)
70. Svensson a, Nicklasson E, Harrah T, Panilaitis B, Kaplan DL, Brittberg M, et al. Bacterial cellulose as a potential scaffold for tissue engineering of cartilage. *Biomaterials*. 2005; 26: 419–31. doi: [10.1016/j.biomaterials.2004.02.049](https://doi.org/10.1016/j.biomaterials.2004.02.049) PMID: [15275816](https://pubmed.ncbi.nlm.nih.gov/15275816/)
71. Helenius G, Bäckdahl H, Bodin A, Nannmark U, Gatenholm P, Risberg B. *In vivo* biocompatibility of bacterial cellulose. *J Biomed Mater Res Part A*. 2006; 76A: 431–438. doi: [10.1002/jbm.a.30570](https://doi.org/10.1002/jbm.a.30570)
72. Tischer PCSF, Sierakowski MR, Westfahl H, Tischer CA. Nanostructural reorganization of bacterial cellulose by ultrasonic treatment. *Biomacromolecules*. 2010; 11: 1217–24. doi: [10.1021/bm901383a](https://doi.org/10.1021/bm901383a) PMID: [20369885](https://pubmed.ncbi.nlm.nih.gov/20369885/)
73. Klemm D, Schumann D, Udhardt U, Marsch S. Bacterial synthesized cellulose artificial blood vessels for microsurgery. *Prog Polym Sci*. 2001; 26: 1561–1603.
74. Klemm D, Heublein B, Fink HP, Bohn A. Cellulose: fascinating biopolymer and sustainable raw material. *Angew Chem Int Ed Engl*. 2005; 44: 3358–93. doi: [10.1002/anie.200460587](https://doi.org/10.1002/anie.200460587) PMID: [15861454](https://pubmed.ncbi.nlm.nih.gov/15861454/)
75. Ishihara K, Nakabayashi N, Fukumoto K AJ. Improvement of blood compatibility on cellulose dialysis membrane. *Biomaterials*. 1992; 13: 145–149. PMID: [1567938](https://pubmed.ncbi.nlm.nih.gov/1567938/)
76. Gibson LJ. The hierarchical structure and mechanics of plant materials. *J R Soc Interface*. 2012; 9: 2749–2766. doi: [10.1098/rsif.2012.0341](https://doi.org/10.1098/rsif.2012.0341) PMID: [22874093](https://pubmed.ncbi.nlm.nih.gov/22874093/)
77. Derda R, Laromaine A, Mammoto A, Tang SKY, Mammoto T, Ingber DE, et al. Paper-supported 3D cell culture for tissue-based bioassays. *PNAS*. 2009; 106: 18457–62. doi: [10.1073/pnas.0910666106](https://doi.org/10.1073/pnas.0910666106) PMID: [19846768](https://pubmed.ncbi.nlm.nih.gov/19846768/)
78. Bhattacharya M, Malinen MM, Lauren P, Lou Y-RR, Kuisma SW, Kanninen L, et al. Nanofibrillar cellulose hydrogel promotes three-dimensional liver cell culture. *J Control Release*. Elsevier B.V.; 2012; 164: 291–298. doi: [10.1016/j.jconrel.2012.06.039](https://doi.org/10.1016/j.jconrel.2012.06.039) PMID: [22776290](https://pubmed.ncbi.nlm.nih.gov/22776290/)
79. Brown EE, Hu D, Abu Lail N, Zhang X. Potential of Nanocrystalline Cellulose–Fibrin Nanocomposites for Artificial Vascular Graft Applications. *Biomacromolecules*. American Chemical Society; 2013; 14: 1063–1071. doi: [10.1021/bm3019467](https://doi.org/10.1021/bm3019467) PMID: [23421631](https://pubmed.ncbi.nlm.nih.gov/23421631/)
80. Dugan JM, Collins RF, Gough JE, Eichhorn SJ. Oriented surfaces of adsorbed cellulose nanowhiskers promote skeletal muscle myogenesis. *Acta Biomater*. 2013; 9: 4707–15. doi: [10.1016/j.actbio.2012.08.050](https://doi.org/10.1016/j.actbio.2012.08.050) PMID: [22963849](https://pubmed.ncbi.nlm.nih.gov/22963849/)
81. Lin N, Dufresne A. Nanocellulose in biomedicine: Current status and future prospect. *Eur Polym J*. Elsevier Ltd; 2014; 59: 302–325. doi: [10.1016/j.eurpolymj.2014.07.025](https://doi.org/10.1016/j.eurpolymj.2014.07.025)
82. Nimeskern L, Hector MA, Sundberg J, Gatenholm P, Muller R, Stok KS. Mechanical evaluation of bacterial nanocellulose as an implant material for ear cartilage replacement. *J Mech Behav Biomed Mater*. 2013; 22: 12–21. Available: http://resolver.scholarsportal.info/resolve/17516161/v22icomplete/12_meobnaimfecr.xml doi: [10.1016/j.jmbbm.2013.03.005](https://doi.org/10.1016/j.jmbbm.2013.03.005) PMID: [23611922](https://pubmed.ncbi.nlm.nih.gov/23611922/)
83. Lu Y, Tekinalp HL, Eberle CC, Peter W, Naskar AK, Ozcan S. Nanocellulose in polymer composites and biomedical applications. *TAPPI J. TECH ASSOC PULP PAPER IND INC, 15 TECHNOLOGY PARK SOUTH, NORCROSS, GA 30092 USA*; 2014; 13: 47–54. Available: http://apps.webofknowledge.com/full_record.do?product=WOS&search_mode=CitingArticles&qid=10&SID=2Aza7k6KmlMONuVr8lZ&page=1&doc=9&cacheurlFromRightClick=no
84. Trindade R, Albrektsson T, Tengvall P, Wennerberg A. Foreign Body Reaction to Biomaterials: On Mechanisms for Buildup and Breakdown of Osseointegration. *Clin Implant Dent Relat Res*. 2014; 1–12. doi: [10.1111/cid.12274](https://doi.org/10.1111/cid.12274)

85. Onuki Y, Bhardwaj U, Papadimitrakopoulos F, Burgess DJ. A review of the biocompatibility of implantable devices: current challenges to overcome foreign body response. *J diabetes Sci Technol*. 2008; 2: 1003–1015. doi: [10.1016/S0091-679X\(07\)83003-2](https://doi.org/10.1016/S0091-679X(07)83003-2) PMID: [19885290](https://pubmed.ncbi.nlm.nih.gov/19885290/)
86. Anderson JM, Rodriguez A, Chang DT. Foreign body reaction to biomaterials. *Semin Immunol*. 2008; 20: 86–100. doi: [10.1016/j.smim.2007.11.004](https://doi.org/10.1016/j.smim.2007.11.004) PMID: [18162407](https://pubmed.ncbi.nlm.nih.gov/18162407/)
87. Jones KS. Effects of biomaterial-induced inflammation on fibrosis and rejection. *Semin Immunol*. 2008; 20: 130–136. doi: [10.1016/j.smim.2007.11.005](https://doi.org/10.1016/j.smim.2007.11.005) PMID: [18191409](https://pubmed.ncbi.nlm.nih.gov/18191409/)
88. Nilsson B, Ekdahl KN, Mollnes TE, Lambris JD. The role of complement in biomaterial-induced inflammation. *Mol Immunol*. 2007; 44: 82–94. doi: [10.1016/j.molimm.2006.06.020](https://doi.org/10.1016/j.molimm.2006.06.020) PMID: [16905192](https://pubmed.ncbi.nlm.nih.gov/16905192/)
89. Motegi K, Nakano Y, Namikawa A. Relation between cleavage lines and scar tissues. *J Maxillofac Surg*. 1984; 12: 21–8. Available: <http://www.ncbi.nlm.nih.gov/pubmed/6583292> PMID: [6583292](https://pubmed.ncbi.nlm.nih.gov/6583292/)
90. Blakeney BA, Tambralli A, Anderson JM, Andukuri A, Lim D-J, Dean DR, et al. Cell infiltration and growth in a low density, uncompressed three-dimensional electrospun nanofibrous scaffold. *Biomaterials*. 2011; 32: 1583–90. doi: [10.1016/j.biomaterials.2010.10.056](https://doi.org/10.1016/j.biomaterials.2010.10.056) PMID: [21112625](https://pubmed.ncbi.nlm.nih.gov/21112625/)
91. Baker BM, Gee AO, Metter RB, Nathan AS, Marklein RA, Burdick JA, et al. The potential to improve cell infiltration in composite fiber-aligned electrospun scaffolds by the selective removal of sacrificial fibers. *Biomaterials*. 2008; 29: 2348–58. doi: [10.1016/j.biomaterials.2008.01.032](https://doi.org/10.1016/j.biomaterials.2008.01.032) PMID: [18313138](https://pubmed.ncbi.nlm.nih.gov/18313138/)
92. Phipps MC, Clem WC, Grunda JM, Clines GA, Bellis SL. Increasing the pore sizes of bone-mimetic electrospun scaffolds comprised of polycaprolactone, collagen I and hydroxyapatite to enhance cell infiltration. *Biomaterials*. 2012; 33: 524–34. doi: [10.1016/j.biomaterials.2011.09.080](https://doi.org/10.1016/j.biomaterials.2011.09.080) PMID: [22014462](https://pubmed.ncbi.nlm.nih.gov/22014462/)
93. Rickert D, Moses MA, Lendlein A, Kelch S, Franke R-P. The importance of angiogenesis in the interaction between polymeric biomaterials and surrounding tissue. *Clin Hemorheol Microcirc*. 2003; 28: 175–81. Available: <http://www.ncbi.nlm.nih.gov/pubmed/12775899> PMID: [12775899](https://pubmed.ncbi.nlm.nih.gov/12775899/)
94. Feng B, Jinkang Z, Zhen W, Jianxi L, Jiang C, Jian L, et al. The effect of pore size on tissue ingrowth and neovascularization in porous bioceramics of controlled architecture *in vivo*. *Biomed Mater*. 2011; 6: 015007. doi: [10.1088/1748-6041/6/1/015007](https://doi.org/10.1088/1748-6041/6/1/015007) PMID: [21206002](https://pubmed.ncbi.nlm.nih.gov/21206002/)
95. Sieminski AL, Gooch KJ. Biomaterial–microvasculature interactions. *Biomaterials*. 2000; 21: 2233–2241. doi: [10.1016/S0142-9612\(00\)00149-6](https://doi.org/10.1016/S0142-9612(00)00149-6)
96. Xiao X, Wang W, Liu D, Zhang H, Gao P, Geng L, et al. The promotion of angiogenesis induced by three-dimensional porous beta-tricalcium phosphate scaffold with different interconnection sizes via activation of PI3K/Akt pathways. *Sci Rep*. 2015; 5: 9409. doi: [10.1038/srep09409](https://doi.org/10.1038/srep09409) PMID: [25797242](https://pubmed.ncbi.nlm.nih.gov/25797242/)
97. Beguin P. The biological degradation of cellulose. *FEMS Microbiol Rev*. 1994; 13: 25–58. doi: [10.1016/0168-6445\(94\)90099-X](https://doi.org/10.1016/0168-6445(94)90099-X) PMID: [8117466](https://pubmed.ncbi.nlm.nih.gov/8117466/)
98. Miyamoto T, Takahashi S, Ito H, Inagaki H, Noishiki Y. Tissue biocompatibility of cellulose and its derivatives. *J Biomed Mater Res*. 1989; 23: 125–133. doi: [10.1002/jbm.820230110](https://doi.org/10.1002/jbm.820230110) PMID: [2708402](https://pubmed.ncbi.nlm.nih.gov/2708402/)
99. Dugan JM, Gough JE, Eichhorn SJ. Bacterial Cellulose Scaffolds and Cellulose Nanowhiskers for Tissue Engineering. *Nanomedicine*. 2013; 8: 297–298.
100. Page H, Flood P, Reynaud EG. Three-dimensional tissue cultures: current trends and beyond. *Cell Tissue Res*. 2013; 352: 123–31. doi: [10.1007/s00441-012-1441-5](https://doi.org/10.1007/s00441-012-1441-5) PMID: [22729488](https://pubmed.ncbi.nlm.nih.gov/22729488/)
101. Behravesh E, Yasko a. W, Engel PS, Mikos a. G. Synthetic Biodegradable Polymers for Orthopaedic Applications. *Clin Orthop Relat Res*. 1999; 367: S118–S129. doi: [10.1097/00003086-199910001-00012](https://doi.org/10.1097/00003086-199910001-00012) PMID: [10546641](https://pubmed.ncbi.nlm.nih.gov/10546641/)
102. Rai R, Keshavarz T, Roether J, Boccaccini A, Roy I. Medium chain length polyhydroxyalkanoates, promising new biomedical materials for the future. *Mater Sci Eng. Elsevier B.V.*; 2011; 72: 29–47. doi: [10.1016/j.mser.2010.11.002](https://doi.org/10.1016/j.mser.2010.11.002)
103. Wang X. Overview on Biocompatibilities of Implantable Biomaterials. *Adv Biomater Sci Appl Biomed*. 2013; 112–154. <http://dx.doi.org/10.5772/53461>
104. Chang H, Wang Y. Cell Responses to Surface and Architecture of Tissue Engineering Scaffolds. *Regen Med Tissue Eng Cells Biomater*. 2011;
105. Sittinger M, Bujia J, Rotter N, Reitzel D, Minuth WW, Burmester GR. Tissue engineering and autologous transplant formation: practical approaches with resorbable biomaterials and new cell culture techniques. *Biomaterials*. 1996; 17: 237–242. doi: [10.1016/0142-9612\(96\)85561-X](https://doi.org/10.1016/0142-9612(96)85561-X) PMID: [8745320](https://pubmed.ncbi.nlm.nih.gov/8745320/)
106. Puschmann TB, Zandén C, De Pablo Y, Kirchoff F, Pekna M, Liu J, et al. Bioactive 3D cell culture system minimizes cellular stress and maintains the *in vivo*-like morphological complexity of astroglial cells. *Glia*. 2013; 61: 432–40. doi: [10.1002/glia.22446](https://doi.org/10.1002/glia.22446) PMID: [23292921](https://pubmed.ncbi.nlm.nih.gov/23292921/)
107. Meinel L, Hofmann S, Karageorgiou V, Kirker-Head C, McCool J, Gronowicz G, et al. The inflammatory responses to silk films *in vitro* and *in vivo*. *Biomaterials*. 2005; 26: 147–155. doi: [10.1016/j.biomaterials.2004.02.047](https://doi.org/10.1016/j.biomaterials.2004.02.047) PMID: [15207461](https://pubmed.ncbi.nlm.nih.gov/15207461/)

108. Torres FG, Commeaux S, Troncoso OP. Biocompatibility of bacterial cellulose based biomaterials. *J Funct Biomater*. 2012; 3: 864–78. doi: [10.3390/jfb3040864](https://doi.org/10.3390/jfb3040864) PMID: [24955750](https://pubmed.ncbi.nlm.nih.gov/24955750/)
109. Cancedda R, Giannoni P, Mastrogiacomo M. A tissue engineering approach to bone repair in large animal models and in clinical practice. *Biomaterials*. 2007; 28: 4240–50. doi: [10.1016/j.biomaterials.2007.06.023](https://doi.org/10.1016/j.biomaterials.2007.06.023) PMID: [17644173](https://pubmed.ncbi.nlm.nih.gov/17644173/)
110. Andrade FK, Silva JP, Carvalho M, Castanheira EMS, Soares R, Gama M. Studies on the hemocompatibility of bacterial cellulose. *J Biomed Mater Res*. 2011; 98: 554–66. doi: [10.1002/jbm.a.33148](https://doi.org/10.1002/jbm.a.33148)
111. McBane JE, Sharifpoor S, Cai K, Labow RS, Santerre JP. Biodegradation and *in vivo* biocompatibility of a degradable, polar/hydrophobic/ionic polyurethane for tissue engineering applications. *Biomaterials*. Elsevier Ltd; 2011; 32: 6034–44. doi: [10.1016/j.biomaterials.2011.04.048](https://doi.org/10.1016/j.biomaterials.2011.04.048) PMID: [21641638](https://pubmed.ncbi.nlm.nih.gov/21641638/)
112. Orlando G, Wood KJ, Stratta RJ, Yoo JJ, Atala A, Soker S. Regenerative medicine and organ transplantation: past, present, and future. *Transplantation*. 2011; 91: 1310–7. doi: [10.1097/TP.0b013e318219ebb5](https://doi.org/10.1097/TP.0b013e318219ebb5) PMID: [21505379](https://pubmed.ncbi.nlm.nih.gov/21505379/)
113. Nakayama KH, Batchelder CA, Lee CI, Tarantal AF. Decellularized Rhesus Monkey Kidney as a Three-Dimensional Scaffold for Renal Tissue Engineering. *Tissue Eng Part A*. 2010; 16. doi: [10.1089/ten.tea.2009.0602](https://doi.org/10.1089/ten.tea.2009.0602)
114. Santerre JP, Woodhouse K, Laroche G, Labow RS. Understanding the biodegradation of polyurethanes: From classical implants to tissue engineering materials. *Biomaterials*. 2005; 26: 7457–7470. doi: [10.1016/j.biomaterials.2005.05.079](https://doi.org/10.1016/j.biomaterials.2005.05.079) PMID: [16024077](https://pubmed.ncbi.nlm.nih.gov/16024077/)
115. Kim MS, Ahn HH, Shin YN, Cho MH, Khang G, Lee HB. An *in vivo* study of the host tissue response to subcutaneous implantation of PLGA- and/or porcine small intestinal submucosa-based scaffolds. *Biomaterials*. 2007; 28: 5137–43. doi: [10.1016/j.biomaterials.2007.08.014](https://doi.org/10.1016/j.biomaterials.2007.08.014) PMID: [17764737](https://pubmed.ncbi.nlm.nih.gov/17764737/)
116. Andrade F, Alexandre N, Amorim I, Gartner F, Mauricio C, Luis L, et al. Studies on the biocompatibility of bacterial cellulose. *J Bioact Compat Polym*. 2012; 28: 97–112. doi: [10.1177/0883911512467643](https://doi.org/10.1177/0883911512467643)
117. Czaja WK, Young DJ, Kawecki M, Brown RM. The future prospects of microbial cellulose in biomedical applications. *Biomacromolecules*. 2007; 8: 1–12. doi: [10.1021/bm060620d](https://doi.org/10.1021/bm060620d) PMID: [17206781](https://pubmed.ncbi.nlm.nih.gov/17206781/)
118. Watanabe K, Eto Y, Takano S, Nakamori S, Shibai H, Yamanaka S. A new bacterial cellulose substrate for mammalian cell culture. *Cytotechnology*. 1993; 13: 107–114. doi: [10.1007/BF00749937](https://doi.org/10.1007/BF00749937) PMID: [7764575](https://pubmed.ncbi.nlm.nih.gov/7764575/)
119. Schumann DA, Wippermann J, Klemm DO, Kramer F, Koth D, Kosmehl H, et al. Artificial vascular implants from bacterial cellulose: preliminary results of small arterial substitutes. *Cellulose*. 2008; 16: 877–885. doi: [10.1007/s10570-008-9264-y](https://doi.org/10.1007/s10570-008-9264-y)